Journal of Catalysis **200,** 69–78 (2001)
doi:10.1006/jcat.2001.3198, available online at http://www.idealibrary.com on IDEAL®

Selective Ammoxidation of Isobutylene to Methacrylonitrile on a New Family of Crystalline Re–Sb–O Catalysts

Haichao Liu, Hideo Imoto,[1] Takafumi Shido, and Yasuhiro Iwasawa[2]

Department of Chemistry, Graduate School of Science, The University of Tokyo, Hongo, Bunkyo-ku, Tokyo 113-0033, Japan

Received August 10, 2000; revised January 2, 2001; accepted January 7, 2001; published online April 18, 2001

The catalytic properties of a new family of crystalline Re–Sb–O compounds $SbRe_2O_6$, $SbOReO_4 \cdot 2H_2O$, and $Sb_4Re_2O_{13}$ in selective ammoxidation of isobutylene to methacrylonitrile (MAN) have been studied and compared with those of a coprecipitated $SbRe_2O_x$ catalyst, an Sb_2O_3-supported Re_2O_7 catalyst, bulk Re oxides, and bulk Sb oxides. The Re-based catalysts were more or less active for MAN synthesis with selectivities of 47.9–83.6% at 673 K, whereas bulk Sb oxides (Sb_2O_3 and Sb_2O_4) showed no activity. The results demonstrate that Re is prerequisite for the ammoxidation catalysis of Re–Sb–O systems. In catalytic systems the presence of Sb also contributes to the ammoxidation catalysis for MAN synthesis. Among these catalysts, $SbRe_2O_6$ was most active and selective (83.6%) for MAN formation at 673 K. No structural change in the bulk and surface of $SbRe_2O_6$ was observed after i-C_4H_8 ammoxidation by means of X-ray diffraction, X-ray photoelectron spectroscopy, scanning electron microscopy, and confocal laser Raman microspectroscopy. The good performance of $SbRe_2O_6$ may be ascribed to its specific crystal structure composed of alternate octahedral $(Re_2O_6)^{3-}$ and $(SbO)^+$ layers. Pulse reaction results suggested that adsorbed NH_3 species on the $SbRe_2O_6$ catalyst facilitated the adsorption and subsequent activation of isobutylene. Increasing reaction temperature and decreasing GHSV did not give rise to increasing formation of by-products CO_2 and acetonitrile, while increasing the i-C_4H_8 conversion. Thus the crystalline $SbRe_2O_6$ compound may be a new promising catalyst for ammoxidation of light hydrocarbons.

Key Words: **Re–Sb oxide catalysts; $SbRe_2O_6$; selective ammoxidation; isobutylene; methacrylonitrile; X-ray diffraction; X-ray photoelectron spectroscopy; scanning electron microscopy; Raman; pulse reaction.**

1. INTRODUCTION

Rhenium-based catalysts have received much attention in many industrial processes such as metathesis of alkenes and reforming of petroleum feedstocks. They also have exhibited unique activities in selective hydrogenation of organic compounds, hydrodesulfurization of heavy crude oil, and selective dehydroaromatization of methane to benzene (1–10). As for selective oxidation, however, Re has found hitherto few applications to the oxidation of methanol and ethanol (7, 11–13). Notwithstanding this fact, Re can be a key element in catalytic oxidation processes because Re oxides possess redox properties comparable to those of V, Mo, and W oxides (14), which are extensively employed as main components in various oxidation catalysts (15–21). Such limited uses of Re in selective oxidation reactions are most likely relevant to the instability of Re oxides involving facile volatilization under usual pretreatment and reaction conditions. Therefore, to develop and understand new catalytic properties of Re, it is essential to discover a new Re mixed oxide system in which Re oxides are stabilized by coexisting second metal oxide species.

The survey of numerous catalyst formulations for selective oxidation and ammoxidation of light hydrocarbons nominates Sb as a good element to form mixed oxide phases with Re due to its unique property as a promoter element in many mixed oxides such as V–Sb–O, Sn–Sb–O, Mo–Sb–O, Fe–Sb–O, and U–Sb–O (15–23). In these catalysts, Sb oxides are considered to facilitate the abstraction of an α-hydrogen from hydrocarbon molecules as well as the subsequent oxygen or nitrogen insertion into allylic intermediate species. Our recent results concerning the Pt/SbO_x catalyst for the selective oxidation of isobutane and isobutylene to methacrolein also show that the Sb_6O_{13} suboxide phase formed under the catalytic oxidation conditions contributes to the oxygen insertion into allylic intermediates in a synergetic manner with Pt particles (24–27). These considerations tempted us to endeavor to develop Re-Sb mixed oxides as a new family of selective oxidation catalysts.

Recently, we employed three crystalline Re–Sb mixed oxides—$SbRe_2O_6$ (mixed valent $Re^{4.5+}$, Sb^{3+}), $SbOReO_4 \cdot 2H_2O$ (Re^{7+}, Sb^{3+}), and $Sb_4Re_2O_{13}$ (Re^{7+}, Sb^{3+})—to examine their performance in the selective oxidation of i-C_4H_8 and i-C_4H_{10} to methacrolein (MAL) (28–30). They displayed promising activities, but a problem encountered

[1] Present address: Department of Applied Chemistry, Faculty of Engineering, Utsunomiya University, Yoto, Utsunomiya 321-8585, Japan.

[2] To whom all correspondence should be addressed. Fax: 81-3-5800-6892. E-mail: iwasawa@chem.s.u-tokyo.ac.jp.

0021-9517/01 $35.00

under the catalytic oxidation conditions was partial decomposition of the catalysts, resulting in the loss of Re oxides. More recently, we have found that the catalytic i-C_4H_8 ammoxidation to methacrylonitrile (MAN) proceeds efficiently on $SbRe_2O_6$ without any decomposition of the crystalline compound (31). In this paper, we report the details of the selective i-C_4H_8 ammoxidation catalysis of the three crystalline Re–Sb–O compounds and their characterization by means of X-ray diffraction (XRD), X-ray photoelectron spectroscopy (XPS), scanning electron microscopy (SEM), and *in situ* confocal laser Raman microspectroscopy (LRM).

2. EXPERIMENTAL

2.1. Preparation of Catalysts

Three crystalline Re–Sb–O compounds—$SbOReO_4 \cdot 2H_2O$, $SbRe_2O_6$, and $Sb_4Re_2O_{13}$—were synthesized by procedures similar to those reported previously (13, 28–30, 32, 33). Briefly, $SbOReO_4 \cdot 2H_2O$ was synthesized hydrothermally as follows: Re_2O_7 2.8 g (Soekawa Chemicals, purity >99.99%) was dissolved in deionized water (2 ml) in a Teflon-lined autoclave. To the resultant perrhenic acid solution, 1.7 g of Sb_2O_3 (Soekawa Chemicals, purity >99.99%) was added under vigorous stirring (Sb/Re atomic ratio = 1/1). Afterward, the autoclave was sealed and maintained at 423 K for 24 h and then at room temperature for 6 days. By drying the resultant compound under vacuum at 343 K, $SbOReO_4 \cdot 2H_2O$ was obtained as a white powder. $SbRe_2O_6$ was synthesized through a solid-state reaction between $SbOReO_4 \cdot 2H_2O$ and metallic Re (Soekawa Chemicals, purity >99.99%) in a 9/5 molar ratio at 773 K for 3 days in a sealed silica tube. The black powder obtained was identified to be $SbRe_2O_6$ by XRD and X-ray fluorescence (XRF). The synthesis of $Sb_4Re_2O_{13}$ was conducted similarly to that of $SbRe_2O_6$. A mixture of $SbOReO_4 \cdot 2H_2O$ and Sb_2O_3 in a 2/1 molar ratio was heated at 773 K for 6 days in an evacuated silica tube to yield gray crystals of $Sb_4Re_2O_{13}$. The BET surface area of the three Re–Sb–O compounds was approximately 1 $m^2\ g^{-1}$.

For comparison, an Sb_2O_3-supported Re_2O_7 catalyst (denoted hereinafter as Re_2O_7/Sb_2O_3; Re loading: 10 wt%) was prepared by an impregnation method using an aqueous solution of NH_4ReO_4 (Soekawa Chemicals, purity >99.9%). A coprecipitated $SbRe_2O_x$ catalyst (denoted as copr. $SbRe_2O_x$) was also prepared by a coprecipitation method using an ethanol solution of $ReCl_3$ and $SbCl_3$, followed by washing with water to eliminate the residual Cl from the catalyst.

2.2. Catalytic Performance

Catalytic ammoxidation reactions were carried out at atmospheric pressure in a Pyrex glass fixed-bed flow reactor (6 mm in diameter). The typical composition of reaction feed was 10% i-C_4H_8, 15% NH_3, and 20% O_2, with the balance He (mol%). The catalysis was conducted typically with 0.15 g of catalyst diluted with 1 g of quartz sand to avoid temperature gradients and hot spots in the reactor. Prior to each run, the catalyst was pretreated in a He flow (40 ml min^{-1}) at 673 K for 1 h. Then the reaction feed was introduced into the reactor at a gas hourly space velocity (GHSV) of 20,000 h^{-1} using digital mass-flow controllers. The reactants and products were analyzed using two on-line gas chromatographs equipped with three columns of Unibeads C at 423 K for O_2, CO, and CO_2, Gaskuropack 54 at 423 K for methacrylonitrile and other oxygenates, and VZ-10 at 348 K for i-C_4H_8 and other hydrocarbons. The steady-state kinetic data were collected over the catalysts after 2 h of time-on-stream.

A blank test at 673 K was conducted in an empty reactor as well, and no i-C_4H_8 conversion was observed in the homogenous gas phase of the reactor.

2.3. Pulse Reactions

Pulse reactions on the $SbRe_2O_6$ catalyst were carried out at 673 K in an apparatus in which pulse- and continuous-flow reactions can be alternatively operated at atmospheric pressure, and He was used as carrier gas at a flow rate of 40 ml min^{-1}. After the $SbRe_2O_6$ catalyst (0.15 g) was pretreated at 673 K under He for 1 h, reaction feeds with different compositions were pulsed into the reactor via a six-port gas sampling valve. The volume of each pulse was ca. 1 ml. The products were analyzed using on-line GC.

2.4. Characterization of Catalysts

XRD patterns were measured in air on a Rigaku Miniflex goniometer using Cu$K\alpha$ radiation ($\lambda = 1.5418$ Å) at 30 kV and 15 mA. The 2θ angles were scanned from 5° to 60° at a rate of 2° min^{-1}.

X-Ray photoelectron spectra were recorded on a Rigaku XPS 7000 spectrometer using Mg$K\alpha$ radiation (1253.6 eV) operated at 200 W. The binding energies were referred to the adventitious C 1*s* peak at 284.6 eV. To minimize exposure of the samples to air, after the pretreatments under He or NH_3/He or after the ammoxidation under a mixture of i-C_4H_8/NH_3/O_2/He, the samples were rapidly cooled to room temperature under the gas flow, followed by sealing of the reactor. Then, in a N_2-filled glove box, the samples were pressed into disks and attached to XPS sample holders with thin double-sided tapes, and transferred to the XPS chamber within 1 min.

Scanning electron micrographs were taken on a Hitachi S-4500 microscope equipped with a field emission gun, which was operated at 15 kV and 10 μA. Different places of the samples were measured to obtain common features of SEM images.

LRM images were recorded on a JASCO NRS2100 SA spectrometer equipped with an Ar^+ laser (514.5 nm) and a liquid N_2-cooled CCD detector. The resolution was 5 cm^{-1}, and the laser power was set to 2 mW. Raman shifts for all the samples were measured in the range 1100–185 cm^{-1}. To evaluate the micrometer-scale homogeneity of the surface, about 30 spectra were measured at different spots of a sample. The samples were analyzed *in situ* similarly to those described previously (28).

3. RESULTS

3.1. Catalytic Performance of Different Re–Sb–O Catalysts

Table 1 lists the conversions, reaction rates, and selectivities of three crystalline Re–Sb–O compounds—$SbRe_2O_6$, $SbOReO_4 \cdot 2H_2O$, and $Sb_4Re_2O_{13}$—in i-C_4H_8 ammoxidation at 673 K (GHSV: 20,000 h^{-1}), in which the performance of copr. $SbRe_2O_x$, Re_2O_7/Sb_2O_3, Sb_2O_3, Sb_2O_4, Re_2O_7, ReO_3, and ReO_2, was also listed for comparison. The Re–Sb–O catalysts as well as bulk Re oxides (Re_2O_7, ReO_3, and ReO_2) were more or less active and selective for the ammoxidation of i-C_4H_8 to MAN, whereas bulk Sb oxides (Sb_2O_3 and Sb_2O_4) showed no activity under the identical conditions. Among the samples examined in Table 1, $SbRe_2O_6$ exhibited the best performance. The steady-state i-C_4H_8 conversion was 5.2% and the selectivity to MAN was 83.6% at 673 K.

3.2. Kinetic Behavior on $SbRe_2O_6$

In the selective oxidation of i-C_4H_8 to MAL, the catalytic property of $SbRe_2O_6$ depended largely on the pretreatment atmospheres (28–30). To investigate the effect of pretreatment of $SbRe_2O_6$ on i-C_4H_8 ammoxidation to form MAN, $SbRe_2O_6$ was pretreated at 673 K for 1 h under the following four different atmospheres: 100% He, 15% NH_3 + 85% He (mol%), 20% O_2 + 80% He, or a reaction mixture of 10% i-C_4H_8 + 15% NH_3 + 20% O_2 + 55% He. As shown in Table 2, after the pretreatments under He, NH_3/He, and the reaction feed, the i-C_4H_8 conversions and MAN selectivities at the steady state were nearly the same, whereas the conversion and selectivity were lower with the pretreatment with O_2/He. Hence, the $SbRe_2O_6$ sample subjected to catalytic performance and characterization in this study was pretreated in a flow of He at 673 K.

TABLE 1

Isobutylene Ammoxidation on Different Catalysts at 673 K[a]

	Conversion (%)	Activity (μmol g-cat^{-1} h^{-1})	Selectivity (%)		
			MAN[b]	CH_3CN	CO_2
$SbRe_2O_6$	5.2	3712.8	83.6	6.1	9.8
$SbOReO_4 \cdot 2H_2O$	0.9	642.6	66.8	3.9	29.1
$Sb_4Re_2O_{13}$	1.9	1356.6	70.7	4.6	24.2
copr.$SbRe_2O_x$	1.4	999.6	69.8	11.1	19.1
Re_2O_7/Sb_2O_3	1.2	856.8	76.8	6.8	16.4
Re_2O_7	1.6	1142.4	47.9	13.2	38.9
ReO_3	1.4	999.6	51.9	17.1	31.0
ReO_2	3.1	2213.4	50.6	17.8	31.6
Sb_2O_3	0	0	—	—	—
Sb_2O_4	0	0	—	—	—

[a] i-C_4H_8/NH_3/O_2/He = 10/15/20/55 (mol%); GHSV = 20,000 h^{-1}.
[b] MAN, methacrylonitrile.

TABLE 2

Catalytic Performance of $SbRe_2O_6$ after Different Pretreatments at 673 K[a]

	i-C_4H_8 conversion (%)	Selectivity to MAN[b] (%)
He pretreatment	5.2	83.6
NH_3/He pretreatment	5.8	85.2
Reaction feed pretreatment	6.0	84.5
O_2/He pretreatment	3.1	70.8

[a] i-C_4H_8/NH_3/O_2/He = 10/15/20/55 (mol%); GHSV = 20,000 h^{-1}.
[b] MAN, methacrylonitrile.

Figure 1a shows the conversion in the i-C_4H_8 ammoxidation on $SbRe_2O_6$ at 673 K as a function of time-on-stream

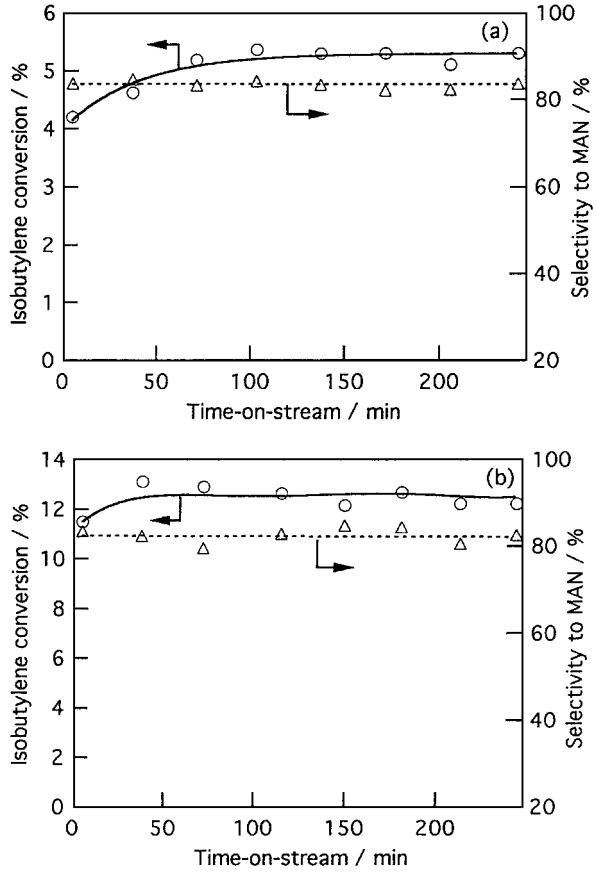

FIG. 1. Reaction profiles of i-C_4H_8 conversion (○) and selectivity to MAN (△) with time-on-stream on $SbRe_2O_6$ at 673 K under GHSV of 20,000 h^{-1} (a) and 10,000 h^{-1} (b).

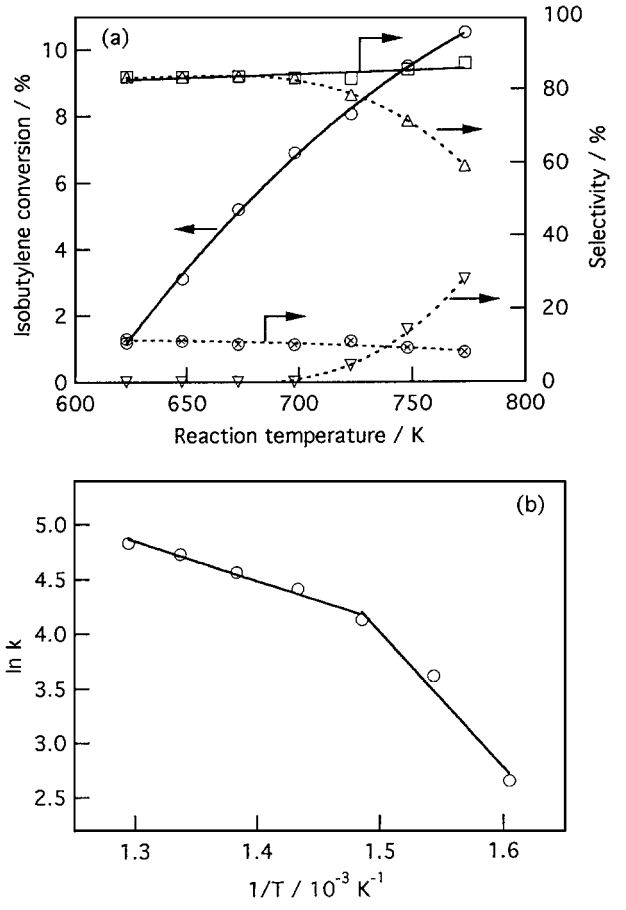

FIG. 2. (a) Catalytic performance of $SbRe_2O_6$ in i-C_4H_8 ammoxidation as a function of reaction temperature. ○, i-C_4H_8 conversion; □, selectivity to MAN + MAL; △, selectivity to MAN; ▽, selectivity to MAL; ⊗, selectivity to CO_2. (b) Arrhenius plot of ln k against T^{-1} for i-C_4H_8 ammoxidation.

at GHSV of 20,000 h^{-1}. It was found that the conversion of i-C_4H_8 initially increased slightly with time and then reached a constant value at 5.2%. The selectivity to MAN remained almost unchanged at 83.6% during the test. When the GHSV decreased to 10,000 h^{-1}, the i-C_4H_8 conversion increased to 12.4%, while the selectivity to MAN (82.6%) did not change so much as compared with that at the GHSV of 20,000 h^{-1} as shown in Fig. 1b.

Figure 2a shows the variation of the conversion and selectivity of the i-C_4H_8 ammoxidation with reaction temperature in the range 623–773 K. i-C_4H_8 conversion increased with increasing temperature, while keeping the MAN selectivity at 83–84% up to 698 K. Above 700 K, another selective oxidation product, MAL, appeared in addition to MAN. The selectivity to MAL reached 28% at 773 K. As a result, the selectivity to MAN decreased above 723 K, while the total selectivity to the sum of MAL + MAN increased slightly. By-products acetonitrile and CO_2 tended to decrease above 723 K, which is an advantageous property of $SbRe_2O_6$. The Arrhenius plots for the i-C_4H_8 conversion rate are shown in Fig. 2b, where there is a break: 103 kJ mol^{-1} at $T < 673$ K and 35 kJ mol^{-1} at $T > 673$ K.

The dependencies of the reaction rate and selectivity on the partial pressure of i-C_4H_8, NH_3, and O_2 at constant GHSV (20,000 h^{-1}) are shown in Fig. 3. At low partial

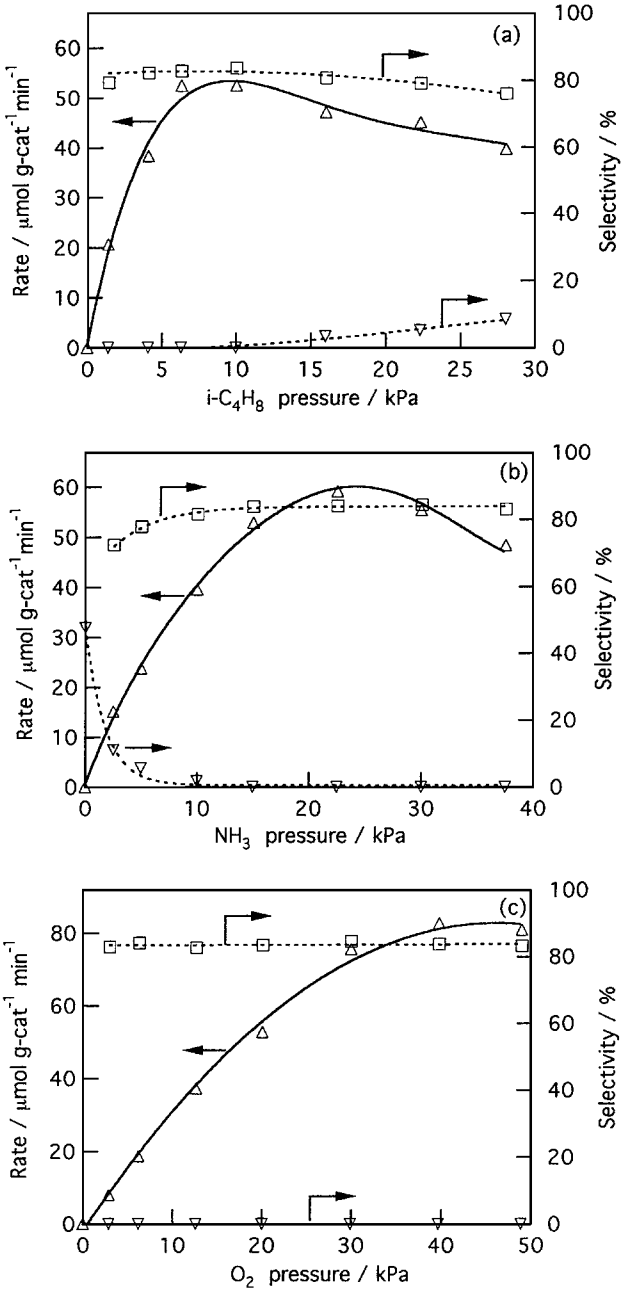

FIG. 3. Catalytic i-C_4H_8 ammoxidation on $SbRe_2O_6$ at 673 K as a function of (a) partial pressure of i-C_4H_8 (15% NH_3, 20% O_2, balance He), (b) partial pressure of NH_3 (10% i-C_4H_8, 20% O_2, balance He), and (c) partial pressure of O_2 (10% i-C_4H_8, 15% NH_3, balance He). △, Reaction rate for MAN formation; □, selectivity to MAN; ▽, selectivity to MAL.

pressures of i-C_4H_8, the rate of MAN formation nearly increased linearly with increasing pressure. After passing through a maximum value around 10 kPa, the rate decreased with a further increase in i-C_4H_8 pressure. As the i-C_4H_8 pressure was higher than 15 kPa, MAL was formed and its selectivity increased from 0 to 8.5% with increasing pressure. Inversely, the selectivity to MAN decreased at the higher i-C_4H_8 pressures, but the selectivity to the sum of MAN + MAL was almost independent of the partial pressure of i-C_4H_8. Similar dependence of the reaction rate on the partial pressure of NH_3 was observed in Fig. 3b where the maximum rate was reached around 22 kPa of NH_3. The selectivity to MAN initially increased and then remained constant with further increasing NH_3 pressure. MAL formation decreased steeply with the increase in NH_3 pressure and eventually reached zero at NH_3 pressures higher than 5 kPa. In contrast to these behaviors in Figs. 3a and 3b, the rate of MAN formation increased with increasing O_2 pressure and attained a saturation value at higher pressures, while selectivity to MAN was almost independent of O_2 pressure in the range 3–50 kPa (Fig. 3c). No MAL was formed under these conditions.

3.3. Pulse Reactions

Four types of pulse experiments were conducted on the $SbRe_2O_6$ catalyst: (i) pulses of the i-C_4H_8/NH_3/O_2/He (10/15/20/55, mol%) mixture, (ii) pulses of the i-C_4H_8/NH_3/He mixture (10/15/75), (iii) pulses of the i-C_4H_8/O_2/He mixture (10/20/70) on NH_3-pretreated $SbRe_2O_6$, and (iv) pulses of the NH_3/O_2/He mixture (15/20/65) on i-C_4H_8-preadsorbed $SbRe_2O_6$.

Pulsing the mixture of i-C_4H_8/NH_3/O_2/He on a fresh $SbRe_2O_6$ catalyst yielded MAN, and the MAN yield increased with the number of pulses to reach a constant value of ca. 6.5% as shown in Fig. 4. Then the pulse was switched

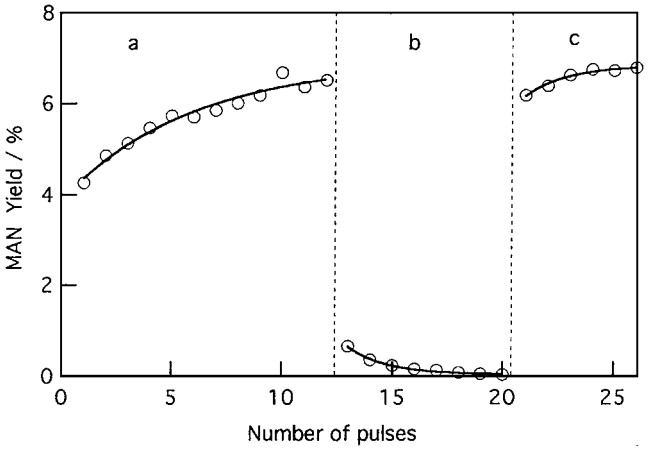

FIG. 4. MAN yields on $SbRe_2O_6$ at 673 K as a function of the number of pulses of i-C_4H_8/NH_3/O_2/He (=10/15/20/55, mol%) (curves a and c) and i-C_4H_8/NH_3/He (=10/15/75) (curve b).

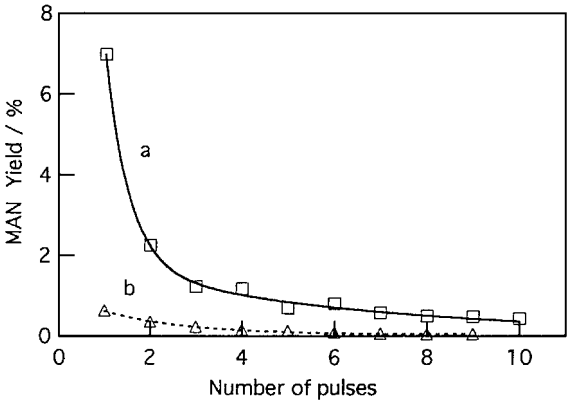

FIG. 5. MAN yields as a function of the number of pulses of i-C_4H_8/O_2/He (=10/20/70, mol%) on NH_3-preadsorbed $SbRe_2O_6$ at 673 K (curve a) and as a function of the number of pulses of NH_3/O_2/He (=15/20/55) on i-C_4H_8-preadsorbed $SbRe_2O_6$ at 673 K (curve b).

to the pulse of i-C_4H_8/NH_3/He mixture without O_2. The MAN yield in the first pulse was as low as 0.7%. MAN formation diminished with further pulses. After i-C_4H_8 conversion became negligible, the i-C_4H_8/NH_3/O_2/He mixture was pulsed into the reactor again, resulting in the recovery of MAN yield as shown in Fig. 4.

Figure 5a shows the MAN yield with i-C_4H_8/O_2/He mixture pulses on the NH_3-pretreated $SbRe_2O_6$ catalyst. A fresh $SbRe_2O_6$ catalyst was treated with NH_3 pulses to saturate the surface with ammonia. The NH_3-saturated catalyst was exposed to the i-C_4H_8/O_2/He pulses. It was found that the first pulse yielded MAN at the high conversion, but the yield decreased sharply by the second and third pulses, followed by a gradual decrease. Figure 5b shows the MAN yield in pulsing a mixture of NH_3/O_2/He on the i-C_4H_8-saturated $SbRe_2O_6$ catalyst. MAN was produced by the reaction of the preadsorbed i-C_4H_8 with NH_3/O_2, but the yield was one order of magnitude lower than the steady-state result.

3.4. Characterization of Catalysts

3.4.1. XRD. Figure 6 shows XRD patterns of the $SbRe_2O_6$ catalyst before and after the pretreatments under He and NH_3/He at 673 K, as well as after i-C_4H_8 ammoxidation reactions at 673 and 773 K for 3 h. It was found that the XRD patterns after these treatments and the i-C_4H_8 ammoxidation were identical to that for the fresh sample. Figure 7 shows XRD patterns of $Sb_4Re_2O_{13}$ and $SbOReO_4 \cdot 2H_2O$ before and after i-C_4H_8 ammoxidation at 673 K. For $Sb_4Re_2O_{13}$, the XRD pattern did not change essentially after the i-C_4H_8 ammoxidation at 673 K for 3 h, but a new peak appeared at a 2θ angle of 27.8°. The new peak was attributable to Sb_2O_3. A dramatic change in crystal structure was observed with $SbOReO_4 \cdot 2H_2O$ after the i-C_4H_8 ammoxidation at 673 K as shown by the XRD

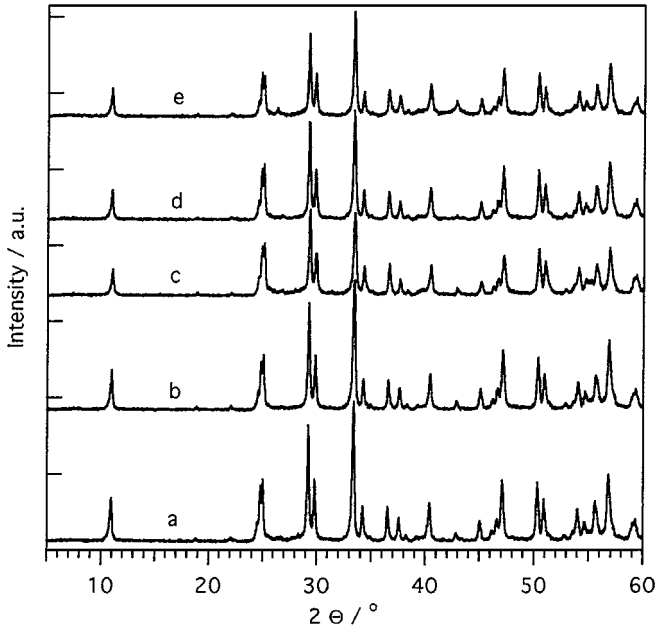

FIG. 6. XRD patterns for $SbRe_2O_6$ before (a) and after pretreatments under He (b) and NH_3/He (c) at 673 K for 1 h and i-C_4H_8 ammoxidation at 673 K (d) and 773 K (curve e) for 3 h.

patterns in Fig. 7 (a and c). The XRD pattern in Fig. 7c was similar to that for $Sb_4Re_2O_{13}$ after that ammoxidation (Fig. 7d).

3.4.2. XPS spectra. Figure 8 shows Re 4*f* XPS spectra for the $SbRe_2O_6$ catalysts before and after the pretreatments with He and NH_3/He at 673 K, as well as after the i-C_4H_8 ammoxidation at 673 and 773 K. In Fig. 8a for fresh $SbRe_2O_6$ three peaks were observed at binding energies of 42.3, 44.8, and 47.7 eV. The peak at 42.3 eV is assigned to Re $4f_{7/2}$ for Re^{4+}. The peak at 47.7 eV is assigned to Re $4f_{5/2}$ probably for Re^{6+} as discussed hereafter. Thus the most intense peak around 44.8 eV should be superimposed by Re $4f_{5/2}$ of Re^{4+} and Re $4f_{7/2}$ of Re^{6+}. We have deconvoluted the XPS spectra as shown in Fig. 8. The Re^{4+} $4f_{5/2}$ and Re^{6+} $4f_{7/2}$ peaks were separated at 44.7 and 45.3 eV, respectively. The $SbRe_2O_6$ sample after pretreatment under He at 673 K exhibited no significant difference from the XPS spectra for the fresh sample. After treatment with NH_3/He at 673 K for 1 h, the intensity of the peaks at 47.7 and 45.3 eV decreased, while the intensity of the peaks at 44.7 and 42.3 eV increased relatively (Fig. 8c). The XPS spectra for the samples after i-C_4H_8 ammoxidation at 673 and 773 K for 3 h were similar to those for the fresh and He-treated samples (Figs. 8d and 8e). The spectra for fresh $SbOReO_4 \cdot 2H_2O$ and $Sb_4Re_2O_{13}$ were similar, exhibiting two peaks centered at 45.7 and 48.1 eV. The peaks are attributable to the Re $4f_{7/2}$ and Re $4f_{5/2}$ levels of Re^{7+} species, respectively. After the ammoxidation reaction at 673 K for 3 h, the spectra changed drastically to show three peaks at 42.3, 44.9, and 47.4 eV. We have deconvoluted the spectra by assuming Re^{6+} and Re^{4+} species, but the fitting has never

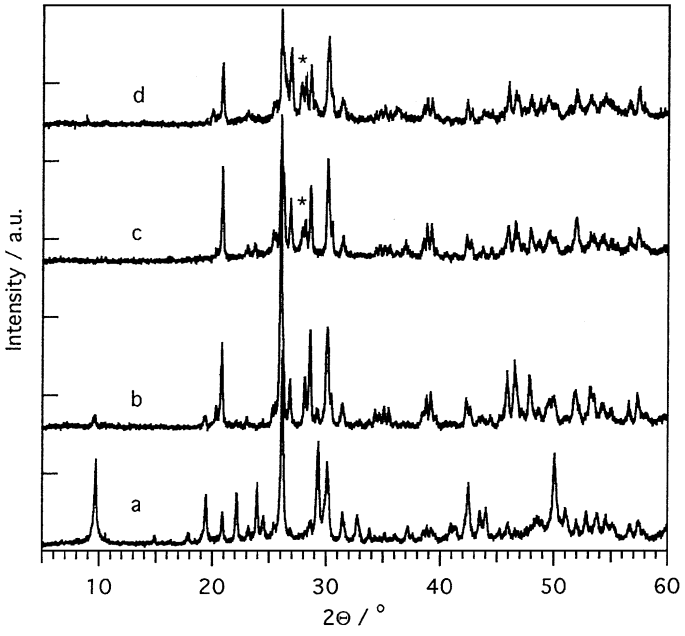

FIG. 7. XRD patterns for fresh $SbOReO_4 \cdot 2H_2O$ (a) and $Sb_4Re_2O_{13}$ (b) and for $SbOReO_4 \cdot 2H_2O$ (c) and $Sb_4Re_2O_{13}$ (d) after i-C_4H_8 ammoxidation at 673 K for 3 h. The asterisks show the XRD peak for the Sb_2O_3 phase.

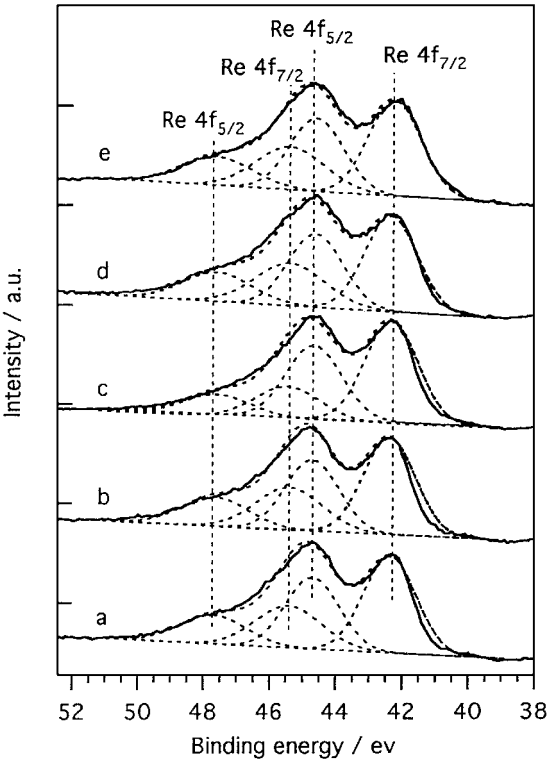

FIG. 8. Re 4*f* XPS spectra for $SbRe_2O_6$ before (curve a) and after pretreatment under He (curve b) and NH_3/He (curve c) at 673 K for 1 h and i-C_4H_8 ammoxidation at 673 K (curve d) and 773 K (curve e) for 3 h.

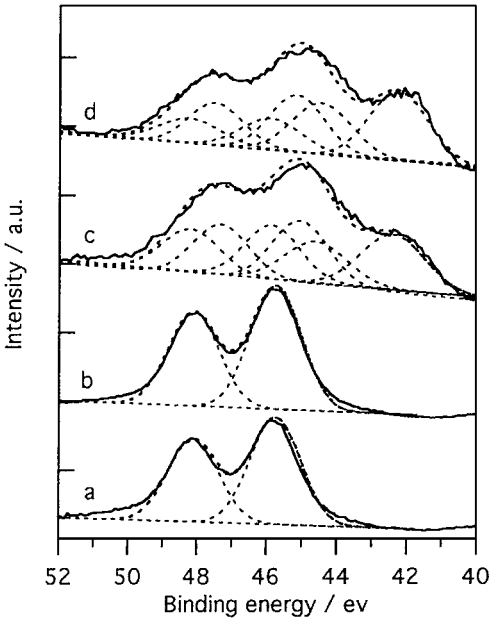

FIG. 9. Re 4*f* XPS spectra for fresh $SbOReO_4 \cdot 2H_2O$ (curve a) and $Sb_4Re_2O_{13}$ (curve b) and for $SbOReO_4 \cdot 2H_2O$ (curve c) and $Sb_4Re_2O_{13}$ (curve d) after i-C_4H_8 ammoxidation at 673 K for 3 h.

reproduced the observed spectra. As a consequence, the fitting has been performed by assuming three different oxidation states of Re. The results are shown in Figs. 9c and 9d. The deconvoluted peaks at 42.3 and 44.7 eV are assigned to Re $4f_{7/2}$ and Re $4f_{5/2}$ peaks for Re^{4+}, respectively, the peaks at 45.1 and 47.5 eV are assigned to Re $4f_{7/2}$ and Re $4f_{5/2}$

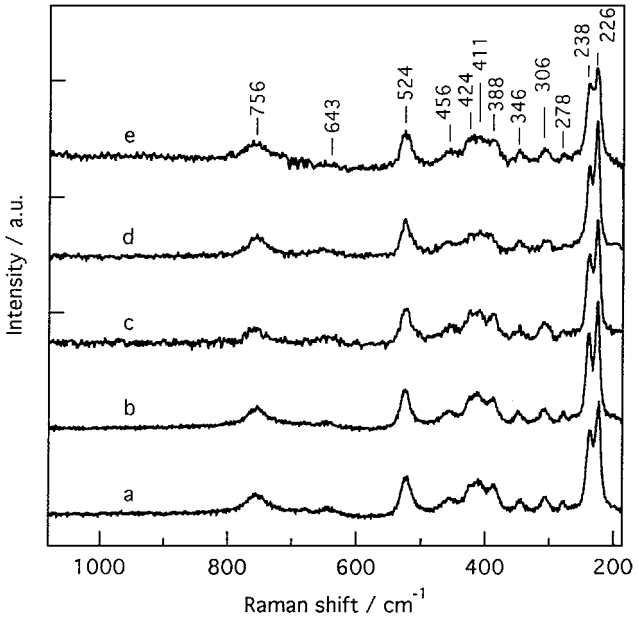

FIG. 10. *In situ* confocal laser Raman microspectra for fresh $SbRe_2O_6$ (curve a) and for $SbRe_2O_6$ after pretreatment under He (curve b) and NH_3/He (curve c) at 673 K for 1 h and i-C_4H_8 ammoxidation at 673 K (curve d) and 773 K (curve e) for 3 h.

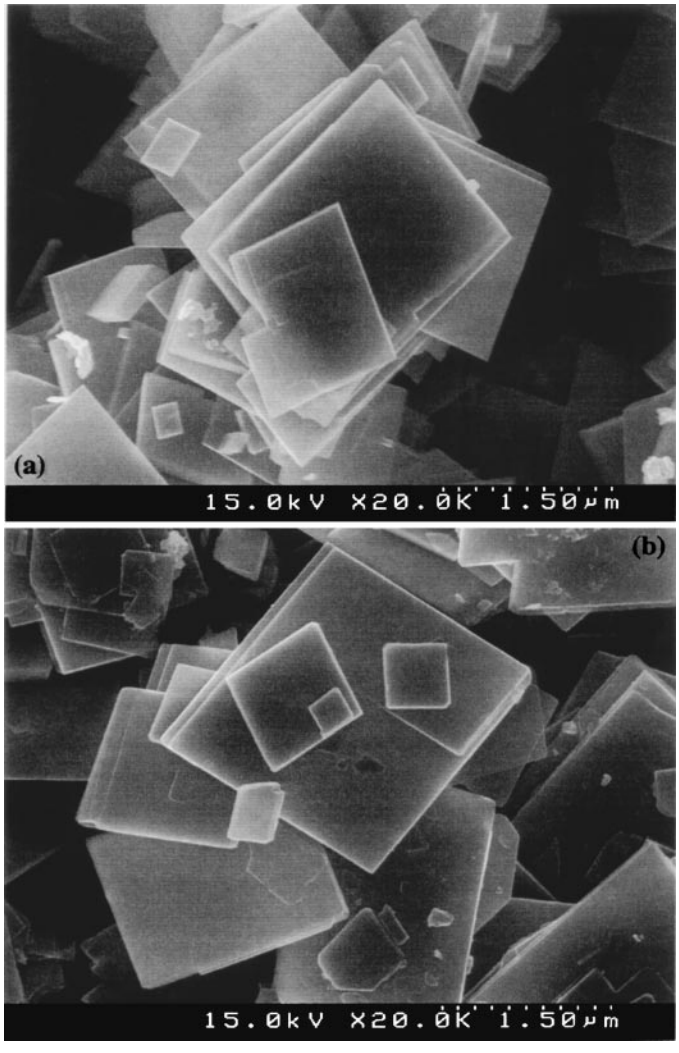

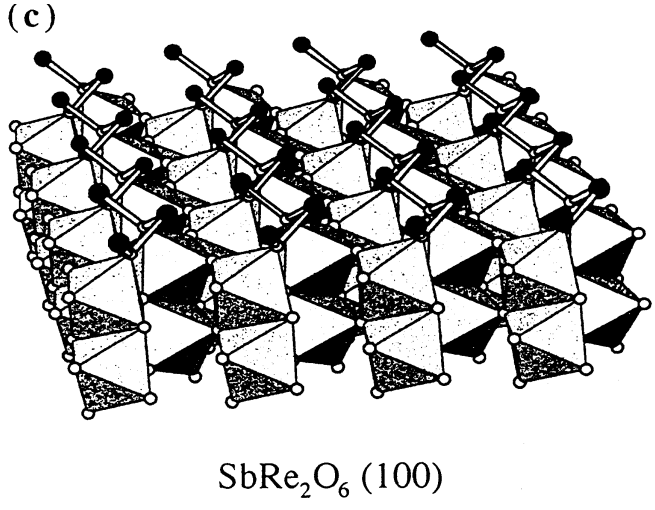

FIG. 11. Scanning electron micrographs for fresh $SbRe_2O_6$ (a) and for $SbRe_2O_6$ after i-C_4H_8 ammoxidation at 673 K for 3 h (b). (c) Drawing of $SbRe_2O_6$ (100) plane.

peaks for Re^{6+}, and the peaks at 45.9 and 48.3 eV are assigned to Re $4f_{7/2}$ and Re $4f_{5/2}$ peaks for Re^{7+}, respectively. It is to be noted that for the three Re–Sb–O compounds Sb 4*d* and Sb $3d_{3/2}$ bands appeared around 34.5 and 539.8 eV, respectively, which are the binding energies typical of Sb^{3+}, independent of the pretreatments and the reaction.

3.4.3. LRM spectra. The $SbRe_2O_6$ samples before and after the pretreatments under He and NH_3/He at 673 K, as well as after the i-C_4H_8 ammoxidation at 673 and 773 K, were also investigated by *in situ* LRM. As shown in Fig. 10. The $SbRe_2O_6$ samples possessed Raman features at 226 (most intense peak), 238s, 278w, 306w, 346w, 388m, 411m, 424m, 456w, 524m, 643w, and 756m cm^{-1} in the range 1100–185 cm^{-1}. After the pretreatments under He and NH_3/He, and the i-C_4H_8 ammoxidation, the Raman shifts essentially remained unchanged.

3.4.4. SEM images. Figures 11a and 11b are the scanning electron micrographs for $SbRe_2O_6$ before and after i-C_4H_8 ammoxidation at 673 K. Fresh $SbRe_2O_6$ was composed of crystals possessing square basal faces with dimensions of 0.5–3 μm and about 100 nm thick. The basal (100) faces were smooth and had sharp and regular edges. After the i-C_4H_8 ammoxidation, the $SbRe_2O_6$ crystals exhibited morphology similar to that for the fresh sample.

4. DISCUSSION

It was found that the Re-based oxides such as the three crystalline Re–Sb–O compounds $SbRe_2O_6$, $SbOReO_4 \cdot 2H_2O$, and $Sb_4Re_2O_{13}$, copr.$SbRe_2O_x$, Re_2O_7/Sb_2O_3, and bulk Re oxides, catalyzed the selective ammoxidation of isobutylene to MAN at 673 K, whereas the bulk Sb oxides were completely inactive under identical reaction conditions (Table 1). These results indicate that rhenium in the Re–Sb–O samples is a prerequisite element to the ammoxidation catalysis. On the other hand, by supporting Re_2O_7 on the inert Sb_2O_3 (Re_2O_7/Sb_2O_3), MAN selectivity increased from 47.9 to 76.8%, and the copr. $SbRe_2O_x$ catalyst gave a selectivity (69.8%) that was also higher than those for bulk Re oxides (Re_2O_7, ReO_3, and ReO_2) (47.9–51.9%). The results indicate that the presence of Sb oxide in the samples contributes positively to an increase in the performance of MAN synthesis. Furthermore, among the Re–Sb–O samples, $SbRe_2O_6$ was much superior to other samples in both activity and selectivity. The difference in catalytic performance may provide information on a key structural issue for i-C_4H_8 ammoxidation catalysis of Re–Sb–O samples.

The most active compound $SbRe_2O_6$ ($Re^{4.5+}$, Sb^{3+}) consists of alternate octahedral $(Re_2O_6)^{3-}$ and $(SbO)^+$ layers, which are connected to each other along the (100) plane as shown in Fig. 11c (33). This crystal structure is maintained under the catalytic ammoxidation conditions as evidenced by XRD, XPS, *in situ* LRM, and SEM (Figs. 6, 8, 10, and 11), which reveal neither change nor modification in bulk and surface of $SbRe_2O_6$. Thus the $SbRe_2O_6$ crystal is a promising catalyst for ammoxidation. The fact that the performance of $SbRe_2O_6$ depends on the crystal structure and oxidation state of Re is also confirmed by the decrease in both activity and selectivity of the $SbRe_2O_6$ sample pretreated under O_2/He (Table 2). It has been demonstrated that destruction of the $SbRe_2O_6$ surface takes place by a partial decomposition of $SbRe_2O_6$ to $Sb_4Re_2O_{13}$ and Re_2O_7 under O_2/He at 673 K (28–30).

The crystalline compounds $SbOReO_4 \cdot 2H_2O$ (Re^{7+}, Sb^{3+}) and $Sb_4Re_2O_{13}$ (Re^{7+}, Sb^{3+}) were built up from tetrahedral $(ReO_4)^-$ anions and cationic $(SbO)^+$ layers (13, 32). In accordance with their formulas, the XPS spectra in Figs. 9a and 9b show the oxidation states of Re and Sb to be 7+ and 3+, respectively. After i-C_4H_8 ammoxidation at 673 K, the XPS spectra for $SbOReO_4 \cdot 2H_2O$ and $Sb_4Re_2O_{13}$ became complicated ones that were reproduced only by the sum of the $4f_{7/2}$ and $4f_{5/2}$ peaks for Re^{7+}, Re^{6+}, and Re^{4+} species (Figs. 9c and 9d). In addition, Sb_2O_3 was observed by XRD in Fig. 7. It is evident that reduction of the two Re–Sb–O compounds occurred under the ammoxidation conditions. Although the fresh $SbOReO_4 \cdot 2H_2O$ and $Sb_4Re_2O_{13}$ possess Re species in the 7+ oxidation state, they show surface Re species (Re^{6+} and Re^{4+}) similar to those for $SbRe_2O_6$ after ammoxidation at 673 K. Nevertheless, the $SbRe_2O_6$ catalyst was superior to the $SbOReO_4 \cdot 2H_2O$ and $Sb_4Re_2O_{13}$ catalysts. There may be two possible explanations for the difference in their performance. The Sb_2O_3 produced by the decomposition of $SbOReO_4 \cdot 2H_2O$ and $Sb_4Re_2O_{13}$ catalysts may cover the catalyst surfaces, resulting in a decrease in performance. This can explain the low activities of the two catalysts (Table 1). However, the low selectivities compared with that for $SbRe_2O_6$ cannot be explained by the presence of Sb_2O_3 at the surfaces because Sb_2O_3 never contributes to the catalytic process and hence does not change the selectivity much (Table 1). It is more plausible that the difference in catalytic performance of the three crystalline Re–Sb–O catalysts may be due not to the difference in their surface Re oxidation states, but to the difference in their surface structures. This is entirely different from the finding in the selective oxidation of i-C_4H_{10} and i-C_4H_8 to MAL that the activities of the three crystalline Re–Sb–O compounds are ascribed to cooperation between Re_2O_7 and $Sb_4Re_2O_{13}$, both being formed under oxidizing conditions (28–30).

In relation to the importance of the structural property of $SbRe_2O_6$ in i-C_4H_8 ammoxidation, it is noteworthy that while the conversion of i-C_4H_8 on the $SbRe_2O_6$ catalyst increased with increasing temperature, formation of the undesired degradation product acetonitrile and combustion product CO_2 decreased above 723 K (Fig. 2a). Figure 1 also shows that while i-C_4H_8 conversion increased by decreasing GHSV, MAN selectivity did not change significantly. It was

found that steady-state catalytic performance remained almost unchanged without any deactivation over at least 10 h on stream. The catalytic performance was reproduced in the repeated experimental runs. These results demonstrate the potential advantage and characteristic property of the crystalline $SbRe_2O_6$, which provides a promising catalyst for the ammoxidation reaction.

Arrhenius plots (Fig. 2b) showed a break in the line and hence a change in the activation energy E_a between 623- and 773 K: 103 kJ mol^{-1} at $T < 673$ K and 35 kJ mol^{-1} at $T > 673$ K. This reflects a change possibly in the rate-determining step in i-C_4H_8 ammoxidation on $SbRe_2O_6$. At $T < 673$ K, the reaction rate may be limited by activation of a C–H bond in i-C_4H_8 adsorbed at the surface, while the adsorption of i-C_4H_8, NH_3, or O_2 may determine the reaction rate above 673 K. At temperatures higher than 700 K, MAL appeared and the selectivity for its formation increased along with the parallel decrease in selectivity to MAN, while keeping the selectivity to the sum of MAL + MAN almost constant. This may be interpreted as a result of the NH_3 coverage decrease at higher temperatures, thus increasing the probability of oxygen incorporation into the methallyl intermediate to yield MAL. This is in agreement with the result shown in Fig. 3b where MAL was produced at low NH_3 pressures. MAL was also produced at high i-C_4H_8 pressures as shown in Fig. 3a, which indicates that NH_3 adsorption is inhibited by i-C_4H_8 at higher pressures. Conversely, when NH_3 pressure increased above 25 kPa, the ammoxidation rate decreased as shown in Fig. 3b. Thus it is probable that adsorption of i-C_4H_8 and NH_3 takes place competitively at the same sites on the catalyst surface.

It is generally accepted that selective oxidation and ammoxidation of hydrocarbons on mixed metal oxides occur following a Mars–van Krevelen type of redox mechanism in which lattice oxygen atoms react with the hydrogen of hydrocarbons to form water and the consumed lattice oxygen atoms are replenished by gas-phase oxygen (23, 34–36). The important contribution of lattice oxygen to the ammoxidation of i-C_4H_8 to MAN on $SbRe_2O_6$ can be seen in Fig. 4. Because the lattice oxygen atoms are consumed first by reaction with NH_3, which is indeed evidenced by the formation of N_2 and H_2O on pulsing NH_3 or the i-C_4H_8/NH_3/He mixture on $SbRe_2O_6$, the MAN yield for the first pulse of the i-C_4H_8/NH_3/He mixture on the steady-state $SbRe_2O_6$ catalyst was as low as 10% of the steady-state value (Fig. 4). However, when O_2 was introduced into the reactor by pulsing the reaction mixture of i-C_4H_8/NH_3/O_2/He, consumed lattice oxygen atoms were rapidly replenished and steady-state activity was recovered (Fig. 4). The XPS spectra in Fig. 8 also demonstrate partial reduction of Re^{6+} species to Re^{4+} species when $SbRe_2O_6$ is pretreated with NH_3/He at 673 K and recovery of the original species under the ammoxidation reaction conditions, indicating that the reduction and oxidation processes of Re species at the catalyst surface are reversible. The amounts of lattice oxygen atoms consumed in the reactions with NH_3 and with i-C_4H_8 were estimated to be approximately 2.3×10^{17}, which corresponds to about 15% of the surface lattice oxygen atoms (ca. 1.5×10^{18}) of the catalyst (0.15 g), assuming the surface oxygen density to be roughly 10^{19} atoms m^{-2} (37). As the replenishment of the surface oxygen atoms by bulk oxygen atoms at 673 K is slow, the consumed surface oxygen atoms are replenished rapidly by gas-phase oxygen. The gas-phase oxygen does not promote i-C_4H_8 combustion to CO_2 as shown in Fig. 3c. The active oxygen atoms may be bound to the Re^{6+} species that are connected to the Sb^{3+}–O–Sb^{3+} chains at the $SbRe_2O_6$ surface. A portion of the surface oxygen atoms are replaced by NH species under the ammoxidation conditions as suggested by FT-IR (38).

The experiments with the alternating pulses of NH_3 and i-C_4H_8 on $SbRe_2O_6$ in Fig. 5 show that MAN is produced mainly by the i-C_4H_8 pulse after the NH_3 pulse rather than by the NH_3 pulse after the i-C_4H_8 pulse. It is supposed that the adsorption of NH_3 to form Re–NH species on $SbRe_2O_6$ facilitates the adsorption and activation of i-C_4H_8. The proposition also accounts for the observation that the activity of $SbRe_2O_6$ for i-C_4H_8 ammoxidation to MAN in the presence of NH_3 is higher than that for the i-C_4H_8 selective oxidation to MAL in the absence of NH_3 under similar reaction conditions. This is in agreement with the results over Bi–Mo oxide catalysts of Wragg *et al.* (39). The promoting effect of NH_3 is much more significant in isobutane ammoxidation on $SbRe_2O_6$, where no C–H bond breaking of isobutane occurs in the absence of NH_3 (31, 38, 40).

5. CONCLUSIONS

1. The three crystalline Re–Sb–O compounds $SbRe_2O_6$, $SbOReO_4 \cdot 2H_2O$, and $Sb_4Re_2O_{13}$ catalyzed the selective ammoxidation of i-C_4H_8 to MAN at 673 K. $SbRe_2O_6$ was superior to the other two compounds in catalytic performance.

2. The performance of copr. $SbRe_2O_x$ and Re_2O_7/Sb_2O_3 catalysts was much worse than that of the $SbRe_2O_6$ catalyst.

3. Re was prerequisite to the ammoxidation catalysis of Re–Sb–O catalysts, while the presence of Sb also contributed positively to the MAN synthesis.

4. No structural change in the bulk and surface of $SbRe_2O_6$ was observed after i-C_4H_8 ammoxidation. The good performance of $SbRe_2O_6$ may be relevant to its specific crystal structure with alternate octahedral $(Re_2O_6)^{3-}$ and $(SbO)^+$ layers which connect to each other through Re–O–Sb bonds.

5. The i-C_4H_8 ammoxidation on $SbRe_2O_6$ took place by a redox mechanism involving the surface oxygen atoms on Re^{6+}.

6. The adsorption of NH_3 on $SbRe_2O_6$ facilitated the adsorption and activation (C–H bond breaking) of i-C_4H_8.

7. Increasing reaction temperature and decreasing GHSV increased i-C_4H_8 conversion to form MAN, but did not give rise to the increase in the formation of by-products CO_2 and acetonitrile, which marks the crystalline $SbRe_2O_6$ as a promising catalyst for hydrocarbon ammoxidation.

ACKNOWLEDGMENTS

This work was supported by Core Research for Evolutional Science and Technology (CREST) of the Japan Science and Technology Corporation (J.S.T.). The SEM measurements were conducted in the Electron Microbeam Analysis Facility of the Mineralogical Institute, University of Tokyo.

REFERENCES

1. Mol., J. C., *Catal. Today* **51**, 289 (1999).
2. Mol, J. C., and Moulijn, J. A., *Adv. Catal.* **24**, 131 (1975).
3. Okal, J., Kepinski, L., Krajczky, L., and Drozd, M., *J. Catal.* **188**, 140 (1999).
4. Thomas, R., Van Oers, E. M., De Beer, V. H. J., Medema, J., and Moulijn, J. A., *J. Catal.* **67**, 241 (1982).
5. Davenport, W. H., Kollonitsch, V., and Kline, C. H., *Ind. Eng. Chem.* **60**, 10 (1968).
6. Blom, R. H., Kolonitsch, V., and Line, C. H., *Ind. Eng. Chem.* **54**, 17 (1962).
7. Kim, D. S., and Wachs, I. E., *J. Catal.* **141**, 419 (1993).
8. Räty, J., and Pakkanen, T. A., *Catal. Lett.* **65**, 175 (2000).
9. Wang, L., Ohnishi, R., and Ichikawa, M., *J. Catal.* **190**, 276 (2000).
10. Ohnishi, R., Issoh, K., Wang, L., and Ichikawa, M., *Stud. Surf. Sci. Catal.* **130**, 3603 (2000).
11. Jehng, J.-M., Hu, H., Gao, X., and Wachs, I. E., *Catal. Today* **28**, 335 (1996).
12. Wang, C.-B., Cau, Y., and Wachs, I. E., *Langmuir* **15**, 1223 (1999).
13. Harrison, W. T. A., Mcmanus, A. V. P., Kaminsky, A. P., and Cheetham, A. K., *Chem. Mater.* **5**, 1631(1993).
14. Wachs, I. E., Deo, G., Andreini, A., Vuurman, M. A., and de Boer, M., *J. Catal.* **160**, 322 (1996).
15. Grasselli, R. K., *Catal. Today* **49**, 141 (1999).
16. Albonetti, S., Cavani, F., and Trifiro, F., *Catal. Rev.-Sci.-Eng.* **38**, 413 (1996).
17. Centi, G., and Trifiro, F., *Catal. Rev.-Sci. Eng.* **28**, 165 (1986).
18. Nilsson, J., Land-Canovas, A. R., Hansen, S., and Andersson, A., *J. Catal.* **186**, 442 (1999).
19. Nilsson, R. Lindblad, T., and Andersson, A., *J. Catal.* **148**, 501 (1994).
20. Berry, F. J., *Adv. Catal.* **30**, 97 (1981).
21. Moro-oka, Y., and Ueda, *Adv. Catal.* **40**, 233 (1994)
22. Pillep, B., Behrens, P., Schubert, U.-A., Spengler, J., and Knözinger, H., *J. Phys. Chem. B* **103**, 9595 (1999).
23. Zanthoff, H.-W., and Buchhloz, S. A., *Catal. Lett.* **49**, 213 (1997).
24. Inoue, T., Asakura, K., and Iwasawa, Y., *J. Catal.* **171**, 184 (1998).
25. Inoue, T., Asakura, K., and Iwasawa, Y., *J. Catal.* **171**, 457 (1998).
26. Inoue, T., Asakura, K., Li, W., Oyama, S. T., and Iwasawa, Y., *Appl. Catal. A* **165**, 183 (1997).
27. Inoue, T., Oyama, S. T., Imoto, H., Asakura, K., and Iwasawa, Y., *Appl. Catal. A* **191**, 131 (2000).
28. Liu, H., Gaigneaux, E. M., Imoto, H., Shido, T., and Iwasawa, Y., *J. Phys. Chem. B* **104**, 2033 (2000).
29. Gaigneaux, E. M., Liu, H., Imoto, H., Shido, T., and Iwasawa, Y., *Top. Catal.* **11/12**, 185 (2000).
30. Liu, H., Gaigneaux, E. M., Imoto, H., Shido, T., and Iwasawa, Y., *Appl. Catal. A* **202**, 251 (2000).
31. Liu, H., Shido, T., and Iwasawa, Y., *Shokubai* [*Catalysts and Catalysis*] **42**, 70 (2000).
32. Watanabe, H., and Imoto, H., *Inorg. Chem.* **36**, 4610 (1997).
33. Watanabe, H., Imoto, H., and Tanaka, H., *J. Solid State Chem.* **138**, 245 (1998).
34. Mars, P., and van Krevelen, D. W., *Chem. Eng. Sci.* **3**, 41 (1954).
35. Knietzni, K. F., Zanthoff., H. W., and Maier, W. F., *J. Catal.* **188**, 154 (1999).
36. Haber, J., and Turek, W., *J. Catal.* **190**, 320 (2000).
37. Winter, E. R. S., *J. Chem. Soc. A*, 2889 (1968).
38. Liu, H., Shido, T., and Iwasawa, Y., to be published.
39. Wragg, R. D., Ashmore, P. G., and Hocey, J. A., *J. Catal.* **31**, 293 (1973).
40. Liu, H., Shido, T., and Iwasawa, Y., *J. Chem. Soc. Chem. Commun.*, 1881 (2000).